Multiband Phase-Modulated RoF Link With Coherent Detection and Bandpass Sampling

Minghua Cao, Jianqiang Li, *Senior Member, IEEE*, Yitang Dai, Feifei Yin, and Kun Xu, *Member, IEEE*

***Abstract*— Bandpass sampling-based coherent detection of multiband subcarrier multiplexed signals was experimentally demonstrated over phase-modulated radio-over-fiber links. Theoretical analysis and experiments are conducted to evaluate the transmission performance. In addition, for multiband transmission, an effective method for determining the valid analog-to-digital converter sampling frequency ranges is derived to ensure no aliasing in the presence of frequency offset. Two quadrature phase-shift keying subcarrier signals were successfully transmitted and recovered over 50.6-km fiber transmission. The experimental results demonstrate that the bandpass sampling performs error free transmission with ∼9 dB the sensitivity penalty when the sampling rate decreases from 10 to 1 GSa/s. The hardware independence and computational complexity reduction is worth of this performance loss.**

***Index Terms*— Radio-over-fiber, coherent communications, bandpass sampling, fiber optics and optical communications.**

I. Introduction

UNIFYING the various wireless services to a given radio frequency (RF) band or wireless standard is not a real possibility. Therefore, there is a trend to design a flexible and simple multi-band multi-standard infrastructure that supports various wireless communication standards simultaneously [1]–[3]. Moreover, in the sense that multiband services will be built on a common platform, especially for those applications with permanent facilities, the longer lifetime is imperative. Radio-over-fiber (RoF) is a promising technology to achieve this goal, since it can inherently transmit multiband RF signals by using subcarrier multiplexing (SCM) over a single fiber, and it enables centralized topology that is convenient in processor and memory upgrading [4].

One of the challenges associated with SCM in RoF links is transceiver linearity, which can severely limit the system dynamic range and thereby degrade system performance. Another challenge is simultaneous frequency down-conversion of multiband RF signals. The superheterodyne arrangement is traditionally considered as standard solutions. Unfortunately, it is inappropriate for multiband transmission because of its difficulty in simultaneously down-conversion of several distinct bands to zero and low-IF frequency band. Even when using the parallel scheme for each single band, the bandpass filters are still an obstacle because the filters are often the most expensive items of the RF modules and have the least flexibility. Additionally, when digitize the signals with analog to digital converter (ADC), if numerous distinct signals are to be processed at several GHz frequency band, the required sampling rate (f_s) must be larger than twice the highest frequency component to satisfy Shannon-Nyquist theorem. The state-of-the-art in ADC technology will have difficulty in achieving that rate inexpensively. Moreover, it will be a waste to process at this rate for information only appearing within several relatively narrow bands [5].

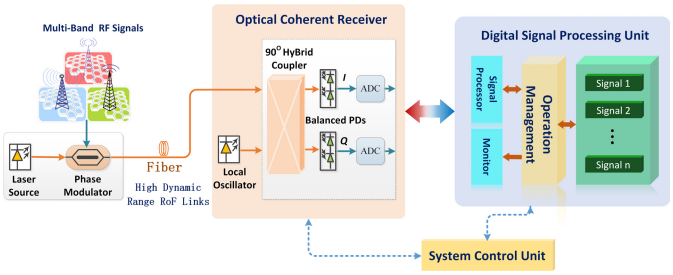

Fig. 1. Schematic diagram of a DSP-aided SCM PM-CD RoF system.

The aforementioned limitations can be overcome through the combination of phase-modulated RoF links with coherent detection (PM-CD RoF) and bandpass sampling with subsequent digital signal processing (DSP), as shown in Fig.1. The PM-CD RoF system has been demonstrated to realize linear transport and to offer advantages in dynamic range and improved power efficiency [6], [7]. In addition, with bandpass sampling, the amount of memory needed to capture a given time interval of incoming signals and the DSP burden can be both reduced. Moreover, direct bandpass sampling takes advantage of eliminating the use of analogue filters and mixers and thereby offers significant power savings [8].

II. Theoretical Analysis of SCM PM-CD RoF Link

In the proposed DSP-aided SCM PM-CD RoF system, the continuous wave (CW) optical carrier can be described as

$$E_{OC}(t) = \sqrt{P_{Sig}} e^{j(w_o t + \theta_o(t))} \quad (1)$$

where P_{Sig} denotes the input optical power, w_o denotes the optical carrier frequency, and θ_o denotes the initial

Manuscript received May 1, 2015; revised July 23, 2015; accepted July 26, 2015. Date of publication August 6, 2015; date of current version September 29, 2015. This work was supported in part by the National Natural Science Foundation of China Program under Grant 61431003, Grant 61302086, Grant 61265003, and Grant 61465007, in part by the Natural Science Foundation for Young Scientists of Gansu Province under Grant 1310RJYA010, and in part by the Specialized Research Fund for the Doctoral Program of Higher Education under Grant 20130005120007.

M. Cao is with the State Key Laboratory of Information Photonics and Optical Communications, Beijing University of Posts and Telecommunications, Beijing 100876, China, and also with the School of Computer and Communication, Lanzhou University of Technology, Lanzhou 730050, China (e-mail: caomh315@163.com).

J. Li, Y. Dai, F. Yin, and K. Xu are with the State Key Laboratory of Information Photonics and Optical Communications, Beijing University of Posts and Telecommunications, Beijing 100876, China (e-mail: jianqiangli@bupt.edu.cn; ytdai@bupt.edu.cn; yff03@139.com; xukun@bupt.edu.cn).

Color versions of one or more of the figures in this letter are available online at http://ieeexplore.ieee.org.

Digital Object Identifier 10.1109/LPT.2015.2462087

signal phase. The incoming multiband RF signals can be written as

$$S_{RF}(t) = \sum_{i=1}^{N} A_i s_i(t) \cos(w_{RF_i} t), \quad i = 1, 2, 3, \cdots \tag{2}$$

where $s_i(t)$ denotes the baseband signals, A_i denotes their amplitude, w_{RF_i} denotes the RF frequency. Therefore, the output of the optical phase modulator can be written as

$$\mathrm{E}_{in}(t) = \sqrt{P_{Sig}} e^{j(w_o t + \theta_o(t))} \cdot e^{jM \sum_{i=1}^{N} A_i s_i(t) \cos(w_{RF_i} t)} \tag{3}$$

where $M = \frac{\pi}{V_\pi}$ is modulation index, V_π is the voltage where the phase modulator generates a π phase shift on the optical signal.

At the receiver side, the optical local oscillator (OLO) laser source can be described as

$$\mathrm{E}_{LO}(t) = \sqrt{P_{LO}} e^{j(w_{LO} t + \theta_{LO}(t))} \tag{4}$$

where P_{LO} is the OLO optical power, w_{LO} and θ_{LO} is the OLO frequency and initial phase. After using a 90° optical hybrid to beat the optical signal with the OLO laser, the outputs are sent to two pairs of balanced photodiodes (BPDs), assume the BPDs are identical, thus, the received signal can be described as

$$s(t) = I_i(t) + j I_q(t) = A_r e^{j(\Delta w(t) + \Delta\theta(t) + M \sum_{i=1}^{N} A_i s_i(t) \cos(w_{RF_i} t))} \tag{5}$$

where $\Delta w(t) = w_o - w_{LO}$, $\Delta\theta = \theta_o - \theta_{LO}$, $A_r = 2R\sqrt{P_{Sig} P_{LO}}$, and R is the responsivity of the BPDs.

Considering the main contributions of the signals are the main and first harmonic components. While neglecting the initial phase difference between the signals and OLO, the second-order and higher order Bessel function magnitude, Eq. (5) can be expand by using Bessel function as

$$\begin{aligned} s(t) &= A_r e^{j\Delta w(t)} e^{jM \sum_{i=1}^{N} A_i s_i(t) \cos(w_{RF_i} t))} \\ &= A_r e^{j\Delta w(t)} \cdot \sum_{i=1}^{N} \sum_{\alpha=-\infty}^{\infty} j^\alpha J_\alpha(M A_i s_i(t)) e^{j\alpha w_{RF_i} t} \\ &\approx A_r e^{j\Delta w(t)} \cdot \sum_{i=1}^{N} (1 - \frac{M^2}{4} A_i^2 s_i^2(t) + j\frac{M}{2} A_i s_i(t) e^{j w_{RF_i} t} \\ &\qquad - j\frac{M}{2} A_i s_i(t) e^{-j w_{RF_i} t}) \end{aligned} \tag{6}$$

Fourier transform of Eq. (6), the result can be described as

$$\begin{aligned} S(w) &= A_r(\delta(w - \Delta w) + \sum_{i=1}^{N} (-\frac{M^2}{16} A_i^2 (S_i * S_i(w - \Delta w))) \\ &\quad + \sum_{i=1}^{N} (j\frac{M}{2} A_i S_i(w - \Delta w - w_{RF_i}) \\ &\qquad - j\frac{M}{2} A_i S_i(w - \Delta w + w_{RF_i})) \end{aligned} \tag{7}$$

where $S_i * S_i(w - \Delta w)$ is the self-convolution of the signals.

It can be extracted that there are two parts in the received signal spectrum. The first centered in Δw which contains the optical carrier and the self-convolution signals. The second centered in $\Delta w \pm w_{RF_i}$, which contains the data. It should be noted that the value of M should be kept within the $(-V_\pi, V_\pi)$ range to avoid phase uncertainty of 2π multiples unless employing phase unwrapping algorithms [9].

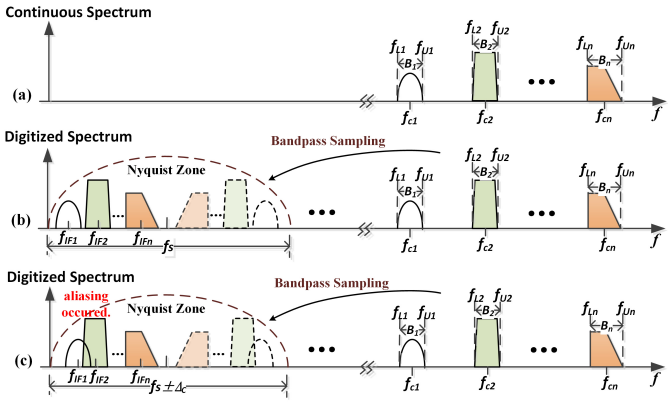

Fig. 2. Simultaneous direct frequency down-conversion for distinct RF signals employing bandpass sampling (a) analog signals in a wideband of interest (b) aliasing-free sampling (c) frequency offset (Δc) caused aliasing.

III. Bandpass Sampling of Multiband Signals

As mentioned, $s(t)$ and $\mathrm{S}(w)$ stand for the time-domain signal and its spectrum. Letting $f_s(t)$ and $F_s(w)$ denote the sampled signal and its spectrum, we will have

$$f_s(t) = \sum_{\mathrm{n}=-\infty}^{\infty} s(t) \cdot \delta(t - nT_s) \tag{8}$$

$$F_s(w) = \frac{1}{T_s} \sum_{n=-\infty}^{\infty} S(w - nw_s), \quad n = 0, \pm 1, \pm 2, \cdots \tag{9}$$

It can be found from Eq. (9) that $F_s(w)$ consists of replicas of $S(w)$ shifted by nw_s. As shown in Fig. 2(b), if sampling at an appropriate rate, the multiband signals will be folded into the first Nyquist zone. It should be noted that there is a challenge in utilizing the bandpass sampling technique to the multiband environment, because the replicas may fold into the interest band and overlap with the desired signals [10]. As a result, an anti-alias scheme is required to avoid aliasing. To find feasible bandpass sampling ranges below the Nyquist rate in a multi-RF-signal coexistence environment for aliasing free sampling, two constraints are imposed which are boundary constraint in the sampled bandwidth and neighbor constraint between adjacent signals [11]. The boundary constraint means that the replicas of signals should be positioned within the sampled bandwidth. The neighbor constraint means that the spectral replicas of different bands must not overlap in the frequency spectrum of the resultant sampled bandwidth.

Assuming that a N-band RF signals are under bandpass sampling, suppose f_s, f_{Hi}, f_{Li}, f_{ci}, f_{IFi} and $B_i (i = 1, 2, \ldots N)$ as the sampling frequency, upper cutoff frequency, lower cutoff frequency, carrier frequency, intermediate frequency (IF) and signal bandwidth, respectively. However, the total number of possible permutations of signal placements is $N! \times 2^N$, so that such a large number of permutations may rather cause a difficulty in finding valid sampling ranges [12]. In order to simplify the analysis, we thus limit the ordering of the given RF signals to one particular case, namely, $f_{c_i} \leq f_{c_{i+1}}$ and $f_{IF_i} \leq f_{IF_{i+1}}$.

To avoid aliasing, the negative frequency part of each signal needs to be located within the frequency range between 0 and $f_s/2$, which can result in $\frac{f_{H_N}}{m_N+0.5} \leq f_s \leq \frac{f_{L_1}}{m_1}$. On the other hand, to avoid overlapping among replicas of down-converted signals, the adjacent signals have the following relations $f_{H_i} - m_i f_s \leq f_{L_{i+1}} - m_{i+1} f_s$. Thus, the valid sampling ranges for multiple signals can be expressed as:

$$\frac{f_{H_N}}{m_N+0.5} \leq f_s \leq min\left\{\frac{f_{L_1}}{m_1}, \cdots, \frac{f_{L_{i+1}} - f_{H_i}}{m_{i+1} - m_i}\right\},$$
$$1 \leq m_i \leq \left\lfloor \frac{f_{L_i}}{2\sum_{i=1}^{N} B_i} \right\rfloor \quad (10)$$

Another challenge to implement coherent receiver with free-running OLO lies in the nonzero frequency offset which pulls the selected operating point to aliasing regions, as shown in Fig. 2(c). As a result, sampling frequency needs careful selection to ensure exact reconstruction of the signals and prevent spectral aliasing upon sampling. Consequently, when taking the varying frequency offset (Δ_c) and sampling jitter (Δ_s) into account, Eq. (10) will be transformed to

$$\frac{f_{H_N} + \Delta_c}{m_N+0.5} + \Delta s \leq f_s$$
$$\leq min\left\{\frac{f_{L_1} - \Delta_c}{m_1} - \Delta s, \cdots, \frac{f_{L_{i+1}} - f_{H_i} - \Delta_c}{m_{i+1} - m_i} - \Delta s\right\} \quad (11)$$

Eq. (11) leads to more accurate and relaxed estimates for actual applications. Note that jitter of modern ADCs usually a tiny fraction of the bit rate of typical wireless communications, so this uncertainty can be negligible for practical sampling rate selection [13]. Thus, ADCs can now be used to digitize the signals at a given sampling rate defined by Eq. (11), and the digitalized signals were then sent to subsequent DSP unit.

IV. Experimental Setup and Results

The main sources of noise that contribute to the signal-to-noise ratio (SNR) of the SCM PM-CD link arise from ADC due to aliasing, jitter and quantization. We have already discussed the effect of ADC and its bit resolution and the system tolerance to laser linewidth in [14]. From a functional view, the incremental improvement in EVM performance at each sampling rate beyond 7 bit resolution is very small. Therefore, a bit resolution of 8 is sufficient to achieve a high performance link for undersampling applications. Similarly, lasers with low linewidth are required in order to get lower EVM. For example, when ADC samples a 2.4 GHz RF signal at 1 GSa/s, lasers with linewidth less than 100 kHz are needed to achieve an EVM below 3% [14]. Therefore, lasers with 100 kHz linewidth are selected to achieve low distortion for the design of high-performance PM-CD link.

The experimental setup for the demonstration of the proposed multiband DSP-aided SCM PM-CD RoF system is shown in Fig. 3. We used two vector signal generator (VSG) to generate multiple quadrature phase shift keying (QPSK) modulated digital data streams. Their bit rates were fixed at 80M and 40M bit/s, respectively. A Nyquist square root raised cosine pulse-shaping filter with 0.25 roll-off factor was applied to limit the signal bandwidth and reduce ISI between symbols.

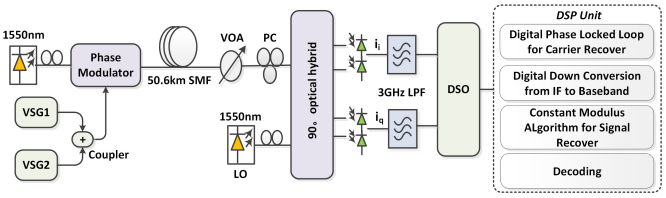

Fig. 3. Experimental set-up for the demonstration of multi-channel SCM PM-CD RoF link.

The generated baseband data signals were respectively modulated on 1.8 GHz and 2.6 GHz carrier frequency and their output power were all set to 0 dBm. The generated RF signals were then combined by a RF coupler to drive the optical phase modulator which supplied with a 100 kHz linewidth CW laser working at 1550 nm. Thereafter, the phase modulated SCM signals were transported to the receiver over 50.6 km long single mode fiber (SMF).

At the receiver side, a 90° optical hybrid was utilized to mix the received optical signal with an OLO laser (ID Photonics CoBrite DX_4), its output power was set as 15 dBm. The 90° optical hybrid output inphase (I) and quadrature (Q) components were then detected using two pairs of BPDs and subsequently digitalized by a digital sampling oscilloscope (DSO, LeCroy 7300A). The digitalized signals can form a vector as described in Eq. (5), which contains all the necessary information to recover the original signals.

Thereafter, DSP techniques were employed to compensate for the channel impairments and demodulate the digitalized photocurrent. First of all, a 2nd-order digital phase-locked loop (DPLL) was utilized to eliminate the frequency offset. In the current demonstration, the frequency offset was measured to be within 240MHz. Fig. 4 shows the DSO sampled signal spectrum before and after DPLL of 10 GSa/s and 1 GSa/s, respectively. It is observed in Fig. 4(a) that the frequency offset push the signal spectrum away from their original location and we can thereby not recover the data. After the DPLL has been applied, the frequency offset has been compensated for. The different channels are clearly observed at their theoretical positions. Likewise, when bandpass sampling, it is evident from Fig. 4(b) that the signals are down-converted to the first Nyquist zone and the free-running OLO caused frequency offset can be successfully removed by the DPLL. After DPLL, the signal was sent to digital down converter (DDC), where the signal down-converted from IF in the first Nyquist zone to baseband. Afterward, constant modulus algorithm (CMA) [15] was used as adaptive equalizer for data convergence. Thereafter, carrier recovery was done including the residual frequency offset estimation based on the fast Fourier transform (FFT) method and carrier phase estimation based on fourth-power Viterbi–Viterbi algorithm. At last, the SCM signals were sent to decoding unit to complete the demodulation.

Fig. 5 illustrates the measured EVM as a function of ADC sampling rates at different received optical power. It demonstrates that the performance degradation of bandpass sampling rate roots in the aggregation of outside band noise into the interest band. This noise power increases roughly by a factor corresponding to the amount of undersampling rate [5]. Thus, the employing of bandpass filters centered on RF carrier frequency with enough bandwidth to accommodate only the

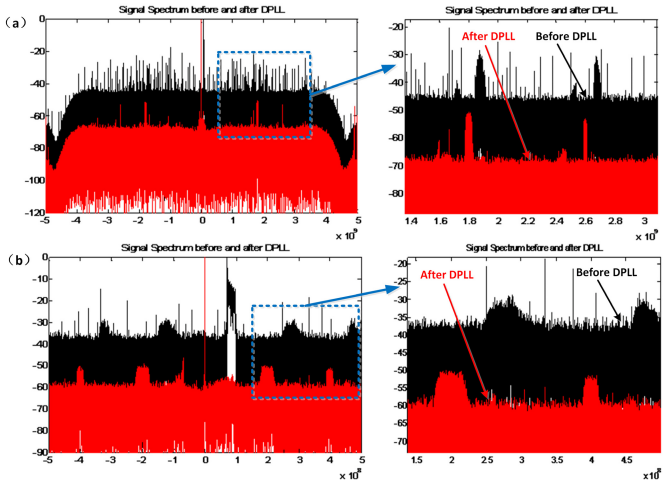

Fig. 4. Signal spectrum before (black) and after (red) DPLL. (a) ADC oversampled at 10 GSa/s, and (b) ADC undersampled at 1 GSa/s.

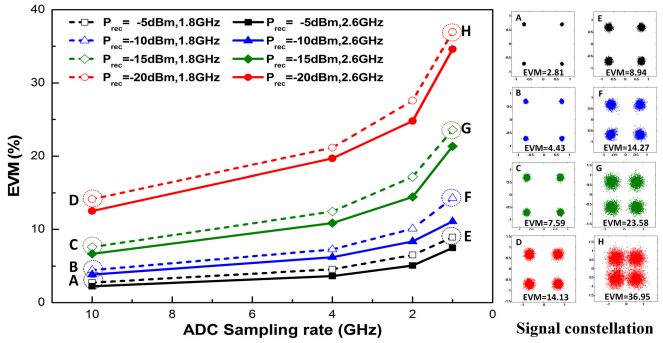

Fig. 5. Measured EVM corresponding to ADC sampling rate and signal constellation of typical values marked with A-H. P_{rec}: received optical power.

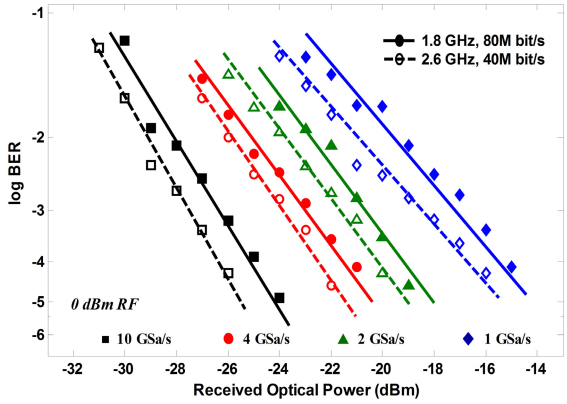

Fig. 6. Experimental BER results for received optical power to the SCM PM-CD RoF link in different sampling rate (50.6km SMF).

data signal by reducing out-of-band noise prior to the ADC is likely to further promote the system performance.

In the experiments, the BER was computed by counting the error bits over a specified period, as shown in Fig. 6. It is evident from the plot that the bit error performance will decline by ~9 dB at the forward error correction (FEC) limit of 2×10^{-3} when ADC sampling rate decreased from 10 GHz to 1 GHz. In view of the received optical power level is not generally the main limiting factor in coherent RoF links because where the fiber link is short, which results in limited attenuation. Therefore, the great reduction of ADCs and DSPs demanding is worth of this performance loss. In addition, we stress that for all of the four sampling rates in both channels, a BER below FEC limit is achieved at which FEC can be used to maintain the error free demodulation. As a result, error free transmission is obtainable in the DSP-aided SCM PM-CD RoF system when using bandpass sampling.

V. Conclusion

In this letter, we extent the work in [14] from single band to multiband transmission, considering the integration of bandpass sampling in DSP-aided SCM PM-CD RoF link to overcome the high sampling rate requirement. The transportation benefits from the advantages of DSP for deficiencies compensation. Despite requiring a complex coherent receiver, we have shown that high-capacity links can be achieved with commercially available optical components. This kind of receiver could potentially be upgraded to operate at higher RF frequencies. The drastic reduction in sampling, processing and memory requirements is attractive for a realistic implementation in microcells. Such a system opens the door for further innovation and simplified networks with an architecture like Soft-RAN [1].

References

[1] A. Gudipati, D. Perry, L. E. Li, and S. Katti, "SoftRAN: Software defined radio access network," in *Proc. HotSDN*, Aug. 2013, pp. 25–30.
[2] Q. Zhang *et al.*, "Multi-service radio-over-fiber system with multiple base-station groups enabled by scalable generation of multi-frequency MMWs," *Opt. Commun.*, vol. 324, pp. 120–126, Aug. 2014.
[3] J. Guillory *et al.*, "WDM-FDM approach for a multiservice home network," in *Proc. OFC*, Mar. 2013, pp. 1–3, paper NTu3J.2.
[4] J. Capmany and D. Novak, "Microwave photonics combines two worlds," *Nature Photon.*, vol. 1, no. 6, pp. 319–330, Jun. 2007.
[5] R. G. Vaughan, N. L. Scott, and D. R. White, "The theory of bandpass sampling," *IEEE Trans. Signal Process.*, vol. 39, no. 9, pp. 1973–1984, Sep. 1991.
[6] T. R. Clark and M. L. Dennis, "Coherent optical phase-modulation link," *IEEE Photon. Technol. Lett.*, vol. 19, no. 16, pp. 1206–1208, Aug. 15, 2007.
[7] D. Zibar, X. Yu, C. Peucheret, P. Jeppesen, and I. T. Monroy, "Digital coherent receiver for phase-modulated radio-over-fiber optical links," *IEEE Photon. Technol. Lett.*, vol. 21, no. 3, pp. 155–157, Feb. 1, 2009.
[8] Y. Yang, C. Lim, and A. Nirmalathas, "Multichannel digitized RF-over-fiber transmission based on bandpass sampling and FPGA," *IEEE Trans. Microw. Theory Techn.*, vol. 58, no. 11, pp. 3181–3188, Nov. 2010.
[9] Y. Pei, J. Yao, K. Xu, J. Li, Y. Dai, and J. Lin, "Advanced DSP technique for dynamic range improvement of a phase-modulation and coherent-detection microwave photonic link," in *Proc. MWP*, Oct. 2013, pp. 72–75.
[10] J. R. G. Oya, A. Kwan, S. A. Bassam, F. Munoz, and F. M. Ghannouchi, "Optimization of subsampling dual band receivers design in nonlinear systems," in *Proc. IEEE MTT-S Int. Microw. Symp.*, Jun. 2012, pp. 1–3.
[11] C.-H. Tseng and S.-C. Chou, "Direct downconversion of multiband RF signals using bandpass sampling," *IEEE Trans. Wireless Commun.*, vol. 5, no. 1, pp. 72–76, Jan. 2006.
[12] J. Bae and J. Park, "An efficient algorithm for bandpass sampling of multiple RF signals," *IEEE Signal Process. Lett.*, vol. 13, no. 4, pp. 193–196, Apr. 2006.
[13] P. Bakopoulos, S. Dris, B. Schrenk, I. Lazarou, and H. Avramopoulos, "Bandpass sampling in heterodyne receivers for coherent optical access networks," *Opt. Exp.*, vol. 20, no. 28, pp. 29404–29412, Dec. 2012.
[14] M. Cao, J. Li, Y. Dai, F. Yin, and K. Xu, "Bandpass sampling based digital coherent receiver with free-running local oscillator laser for phase-modulated radio-over-fiber links," *Opt. Exp.*, vol. 22, no. 22, pp. 27007–27018, Nov. 2014.
[15] A.-J. van der Veen and A. Paulraj, "An analytical constant modulus algorithm," *IEEE Trans. Signal Process.*, vol. 44, no. 5, pp. 1136–1155, May 1996.